Molecular determinants of clinical outcomes of pembrolizumab in recurrent ovarian cancer: exploratory analysis of KEYNOTE-100

Jonathan A. Ledermann[a,*], Ronnie Shapira-Frommer[b], Alessandro D. Santin[c], Alla S. Lisyanskaya[d], Sandro Pignata[e], Ignace Vergote[f], Francesco Raspagliesi[g], Gabe S. Sonke[h], Michael Birrer[i], Diane M. Provencher[j], Jalid Sehouli[k], Nicoletta Colombo[l,m], Antonio González-Martín[n], Ana Oaknin[o], P. B. Ottevanger[p], Vilius Rudaitis[q], Julie Kobie[r], Michael Nebozhyn[r], Mackenzie Edmondson[r], Yuan Sun[r], Razvan Cristescu[r], Petar Jelinic[r], Stephen M. Keefe[r], Ursula A. Matulonis[s]

[a] Department of Oncology, UCL Cancer Institute, University College London, London, United Kingdom

[b] The Ella Lemelbaum Institute for Immuno-Oncology, Sheba Medical Center, Tel HaShomer Hospital, Ramat Gan, Israel

[c] Department of Obstetrics, Gynecology, and Reproductive Sciences, Yale University, New Haven, CT, United States

[d] Department of Oncogynecology, St. Petersburg City Clinical Oncology Dispensary, St. Petersburg, Russia

[e] Department of Urology and Gynecology, Istituto Nazionale Tumori IRCCS Fondazione G. Pascale, Naples Italy

[f] Department of Obstetrics and Gynaecology, Division of Gynecologic Oncology, University Hospital Leuven, Leuven, Belgium

[g] Fondazione IRCCS Istituto Nazionale dei Tumori, Milan, Italy

[h] Department of Medical Oncology, Netherlands Cancer Institute, Amsterdam, Netherlands

[i] UAMS Winthrop P. Rockefeller Cancer Institute, Little Rock, AR, United States

[j] Centre Hospitalier de l'Université de Montréal (CHUM), Institut du Cancer de Montréal, Montreal, Canada

[k] Gynecology with Center of Oncological Surgery, Charité-Medical University of Berlin, Berlin, Germany

[l] Department of Medicine and Surgery, University of Milan-Bicocca, Milan, Italy

[m] European Institute of Oncology, IRCCS, Milan, Italy

[n] Department of Medical Oncology and Program in Solid Tumors-Cima, Cancer Center Clínica Universidad de Navarra, Madrid, Spain [o] Vall d'Hebron University Hospital, Vall d´Hebron Institute of Oncology (VHIO), Barcelona, Spain

[p] Medical Oncology, Radboud University Medical Center, Nijmegen, Netherlands

[q] Clinic of Obstetrics and Gynecology, Vilnius University Institute of Clinical Medicine, Vilnius, Lithuania

[r] Merck & Co., Inc., Rahway, NJ, United States

[s] Division of Medical Oncology, Dana-Farber Cancer Institute, Boston, MA, United States

*****Corresponding author:

Jonathan Ledermann, MD, FMedSci

Department of Oncology

UCL Cancer Institute,

72 Huntley Street

London WC1E 6DD

United Kingdom

Email: j.ledermann@ucl.ac.uk

Phone: +44 20 3108 4261

Keywords (≤6 words): ovarian cancer; pembrolizumab; gene expression signatures; tumor mutational burden; tumor microenvironment cell phenotypes

Target Journal: *Gynecol Oncol*

Main Text [≤ 4000 words]: 3878 (excluding Tables, and Figure legends)

Abstract [≤250 words]: 250

Tables and figures (≤6): 2 tables/4 figures

References (≤40): 32

Supplementary: 1 table/7 figures

HIGHLIGHTS (3-5 bullet points; ≤125 characters each, including spaces)

- Association of molecular determinants with outcomes of pembrolizumab in advanced recurrent ovarian cancer was evaluated. (**122/125**)
- No evidence of associations between ORR and key axes of gene expression was observed with pembrolizumab monotherapy. (**119/125**)
- T-cell–inflamed GEP-adjusted glycolysis and hypoxia signatures were negatively associated with clinical outcomes. **(116/125)**
- Continuous TMB was not associated with efficacy, but TMB ≥175 mut/exome (≈ ≥10 mut/Mb) trended toward improved outcomes. **(123/125)**
- Higher densities of myeloid cell phenotypes CD11c+ and CD11c+/MHCII−/CD163−/CD68− trended toward improved efficacy. **(118/125)**

ABSTRACT (249/≤250 words)

Objective. This prespecified exploratory analysis evaluated the association of gene expression signatures, tumor mutational burden (TMB), and multiplex immunohistochemistry (mIHC) tumor microenvironment–associated cell phenotypes with clinical outcomes of pembrolizumab in advanced recurrent ovarian cancer (ROC) from the phase II KEYNOTE-100 study.

Methods. Pembrolizumab-treated patients with evaluable RNA-sequencing (*n*=317), whole exome sequencing (*n*=293), or select mIHC (*n*=125) data were evaluated. The association between outcomes (objective response rate [ORR], progression-free survival [PFS], and overall survival [OS]) and gene expression signatures (T-cell–inflamed gene expression profile [Tcell$_{inf}$GEP] and 10 non-Tcell$_{inf}$GEP signatures), TMB, and prespecified mIHC cell phenotype densities as continuous variables was evaluated using logistic (ORR) and Cox proportional hazards regression (PFS; OS). One-sided *p*-values were calculated at prespecified α=0.05 for Tcell$_{inf}$GEP, TMB, and mIHC cell phenotypes and at α=0.10 for non-Tcell$_{inf}$GEP signatures; all but Tcell$_{inf}$GEP and TMB were adjusted for multiplicity.

Results. No evidence of associations between ORR and key axes of gene expression was observed. Negative associations were observed between outcomes and Tcell$_{inf}$GEP-adjusted glycolysis (PFS, adjusted-*p*=0.019; OS, adjusted-*p*=0.085) and hypoxia (PFS, adjusted-*p*=0.064) signatures. TMB as a continuous variable was not associated with outcomes (*p*>0.05). Positive associations were observed between densities of myeloid cell phenotypes CD11c^{+} and CD11c^{+}/MHCII^{-}/CD163^{-}/CD68^{-} in the tumor compartment and ORR (adjusted-*p*=0.025 and 0.013, respectively).

Conclusions. This exploratory analysis in advanced ROC did not find evidence for associations between gene expression signatures and outcomes of pembrolizumab. mIHC analysis suggests CD11c^{+} and CD11c^{+}/MHCII^{-}/CD163^{-}/CD68^{-} phenotypes representing

myeloid cell populations may be associated with improved outcomes with pembrolizumab in advanced ROC.

Clinical trial registration: ClinicalTrials.gov, NCT02674061.

1. Introduction

Ovarian cancer is the leading cause of gynecologic cancer–related mortality in women [1]. Guideline-recommended therapies for patients with recurrent epithelial ovarian, fallopian tumor, or primary peritoneal cancer include chemotherapy and single-agent targeted therapies (bevacizumab, niraparib, olaparib, and rucaparib) [2]. Other recommended therapies include anti–programmed cell death 1 (PD-1) monoclonal antibodies dostarlimab-gxly for patients with recurrent or advanced tumors characterized as microsatellite instability-high (MSI-H) or deficient mismatch repair (dMMR) and pembrolizumab for patients with unresectable or metastatic MSI-H/dMMR or tumor mutational burden (TMB)-high (≥10 mutations/megabase) tumors [3,4].

Investigation of clinical outcomes with anti–PD-1/programmed death ligand 1 (PD-1/L1) immunotherapies in patients with recurrent ovarian cancer (ROC) has demonstrated minimal antitumor activity when administered as monotherapy [5-9]. In the 2-cohort, single-arm, phase II KEYNOTE-100 study in patients with advanced ROC who previously received 1–3 (cohort A) or 4–6 (cohort B) prior lines of therapy, pembrolizumab monotherapy demonstrated low antitumor activity in the overall study population (*N* = 376; objective response rate [ORR], 8.0%) [6]. ORR increased with increasing PD-L1 combined positive score (CPS; CPS <1, 5.0%; CPS ≥1, 10.2%; CPS ≥10, 17.1%) and this trend was consistent within both cohorts of the study [6]. Data from tumor samples from patients enrolled in the KEYNOTE-100 study have been previously included in pan-tumor analyses evaluating the association between TMB and gene expression signatures with clinical outcomes of pembrolizumab monotherapy [10-12]. In one such pan-tumor analysis, TMB was found to be significantly associated with clinical outcomes of pembrolizumab, with TMB ≥175 mutations/exome (via whole-exome sequencing [WES]; equivalent to ≥10

mutations/megabase via FoundationOne®CDx [10]) associated with a clinically meaningful improvement in the efficacy of pembrolizumab monotherapy [11]. Gene expression signatures such as the interferon-γ–related 18-gene T-cell–inflamed gene expression profile ($Tcell_{inf}GEP$) and 10 other non-$Tcell_{inf}GEP$ signatures from tumor microenvironment (TME)–associated cell types have been evaluated across several tumor types, with some of these signatures significantly associated with response to pembrolizumab [12].

Myeloid-derived suppressor cells (MDSCs) suppress T-cell responses in the TME, and high infiltration of MDSCs in solid tumors has been shown to correlate with poor response to immune checkpoint inhibitors [13-17]. Recently, multiplex immunohistochemistry (mIHC) analysis of baseline tumors in patients with locally advanced triple-negative breast cancer showed that the density of certain myeloid cell phenotypes within the tumor compartment, including $CD11c^+$ (macrophage and dendritic cell), $CD11c^+/MHCII^+/CD163^-/CD68^-$ (dendritic cell), $CD11c^+/MHCII^-/CD163^-/CD68^-$ (nonactivated/immature dendritic cell), and $CD11c^+/CD163^+$ (M2 macrophage) phenotypes, displayed a promising positive association trend with pathologic complete response following neoadjuvant pembrolizumab plus chemotherapy.

To improve the understanding of immune interactions in the TME and possibly elucidate drivers of pembrolizumab response or/resistance in advanced ROC, we performed an exploratory analysis of KEYNOTE-100 on the association of gene expression signatures ($Tcell_{inf}GEP$ and non-$Tcell_{inf}GEP$ signatures), TMB, and the density of mIHC TME-associated cell phenotypes with clinical outcomes of pembrolizumab.

2. Materials and methods

2.1. Study design, participants, and treatment

Study design and eligibility criteria of the KEYNOTE-100 study (ClinicalTrials.gov identifier: NCT02674061) have been published [6]. Briefly, adult patients with recurrent advanced epithelial ovarian cancer, fallopian tube cancer, or primary peritoneal cancer, disease progression after platinum-based therapy, documented evidence of clinical response or disease stabilization on the last treatment regimen received, measurable disease at baseline per Response Evaluation Criteria in Solid Tumors version 1.1 (RECIST v1.1), Eastern Cooperative Oncology Group (ECOG) performance status of 0 or 1, life expectancy ≥16 weeks, and normal organ function were eligible for the study; archival formalin-fixed paraffin-embedded block specimens of tumor tissue from prior cytoreductive surgery or newly obtained tumor tissue at screening was required. Key exclusion criteria included prior anti–PD-1/L1 therapy.

The study enrolled 2 cohorts. Patients in cohort A had received 1 to 3 prior lines of treatment and had a platinum-free interval (PFI; time elapsed between the last dose of platinum and documented evidence of disease progression per RECIST v1.1) or treatment-free interval (TFI; time elapsed between the last dose of the regimen received and documented evidence of disease progression per RECIST v1.1) of 3 to 12 months based on the last regimen received. Patients in cohort B had received 4 to 6 prior lines of treatment and had a PFI/TFI of ≥3 months based on the last regimen received. In both cohorts, patients received pembrolizumab 200 mg intravenously every 3 weeks for ≤35 cycles (~2 years) or until disease progression, unacceptable toxicity, investigator decision, noncompliance, or patient withdrawal of consent.

The study protocol and all amendments were approved by the institutional review board or ethics committee at each participating institution. The study was conducted in accordance with the protocol, its amendments, the ethical principles originating from the Declaration of Helsinki, and Good Clinical Practice guidelines. Written informed consent was provided by all patients before enrollment.

2.2. Outcomes

The RNA-sequencing objectives for this exploratory analysis were to evaluate the association of the $Tcell_{inf}$GEP and 10 non-$Tcell_{inf}$GEP signatures (angiogenesis, glycolysis, granulocytic MDSC [gMDSC], hypoxia, monocytic MDSC [mMDSC], MYC, proliferation, RAS, stroma/ epithelial-to-mesenchymal transition [EMT]/transforming growth factor-beta [TGF-β], and WNT) as continuous variables with clinical outcomes (ORR, progression-free survival [PFS], and overall survival [OS]) of pembrolizumab. The WES objectives were to evaluate the association between TMB as a continuous variable and clinical outcomes (ORR, PFS, and OS) of pembrolizumab, as well as the impact of TMB on efficacy estimates based on a prespecified cutoff of 175 mutations/exome. The mIHC objectives were to evaluate the association between a prespecified subset of the mIHC cell phenotypes ($CD11c^+$ [macrophage and dendritic cell], $CD11c^+/MHCII^+/CD163^-/CD68^-$ [dendritic cell], $CD11c^+/MHCII^-/CD163^-/CD68^-$ [nonactivated/immature dendritic cell], and $CD11c^+/CD163^+$ [M2 macrophage]) and clinical outcomes (ORR, PFS, and OS) of pembrolizumab, as well as to descriptively evaluate the association of select mIHC cell phenotypes ($Foxp3^+$, $CD8^+/GB^+/Ki67^+$, and $CD11c^+/MHCII^-/CD163^-/CD68^-$; based on high discriminatory ability in the tumor compartment relative to other phenotypes) in the tumor compartment, stromal compartment, and the overall TME with response. The correlations of

densities of mIHC cell phenotypes in tumor compartment and PD-L1 CPS, and densities of mIHC cell phenotypes in tumor compartment and $Tcell_{inf}GEP$, were also evaluated.

2.3. Assessments

RNA-sequencing was performed using the HiSeq 3000/HiSeq 4000 platform (Illumina Inc., CA, USA) on baseline tumor specimens provided during screening. Analysis of the RNA-sequencing raw reads and subsequent gene expression quantification were as previously described [12]. The $Tcell_{inf}GEP$ signature score was calculated as the weighted sum of normalized expression values for 18 genes determined as predictors of response in the pan-tumor setting on the NanoString platform [18]. Scores for the 10 non-$Tcell_{inf}GEP$ signatures were calculated as the average of the consensus genes (on the logarithmic scale) in each signature gene set as previously described [12].

TMB was determined via WES (mutations/exome) of tumor samples and matched DNA. TMB was defined as the number of somatic nonsynonymous single nucleotide variants and indels that met predetermined criteria as previously described [11,19].

TME-associated cell populations of activated and inactive CD8 T cells, CD8 T cells enriched for antigen specificity, total and regulatory T cells, tumor-associated fibroblasts, total and M2 macrophages, and dendritic cells were quantified in baseline tumor samples using mIHC analysis on whole slide images with the Halo software (Indica Labs, Albuquerque, NM; Supplementary Figs. S1 and S2). mIHC was performed using the Vectra Polaris Imaging System (Akoya Biosciences, Marlborough, MA) with two 6-plex panels: activated T-cell panel (CD103/CD39/Granzyme B/CD8/Cytokeratin/Ki67) and modified myeloid/stroma/Treg panel (CD68/CD163/ CD11c/MHCII/FAP/FoxP3). mIHC sample preparation, staining, and quantitative imaging were performed as described in Supplementary Text 1.

The number of positive cells per mm^2 (i.e. density) was calculated for each analyte in the tumor compartment, stromal compartment, and the overall TME. Tumor/stromal compartment classification and analysis algorithm outputs for each stain in each specimen were reviewed by pathologists for quality.

PD-L1 expression was determined using PD-L1 IHC 22C3 pharmDx (Agilent Technologies Inc.). PD-L1 CPS was calculated as the number of PD-L1-staining cells (tumor cells, lymphocytes, and macrophages) divided by the total number of viable tumor cells, multiplied by 100.

Tumor response was assessed by computed tomography or magnetic resonance imaging every 9 weeks for the first 54 weeks, and every 12 weeks thereafter. ORR was defined as the proportion of patients in the analysis population who had a complete response or partial response per RECIST v1.1 by blinded independent central review (BICR). PFS was defined as the time from first dose to the first documented disease progression per RECIST v1.1 by BICR or death due to any cause, whichever occurred first. OS was defined as the time from first dose to death due to any cause.

2.4. Statistical analysis

The analysis population comprised all pembrolizumab-treated patients in the KEYNOTE-100 study with clinical data and evaluable RNA-sequencing data, evaluable WES data, or mIHC (activated T-cell panel or modified myeloid panel) data; the mIHC population was selected to include responders at an ~1:3 ratio of responders to nonresponders matched by histology. Analyses were performed according to a scientific and statistical analysis plan developed prior to merging clinical data with biomarker assessment, specifying where statistical testing would be used and what biomarker cutoffs defined the subgroups.

The association between clinical outcomes and the RNA-based gene expression signature scores, WES-based TMB (log_{10} scale), and the prespecified subset of mIHC cell phenotypes as continuous variables was evaluated using logistic regression (ORR) and Cox proportional hazards regression (PFS and OS), with adjustments for ECOG performance status; the 10 non-$Tcell_{inf}$GEP signatures scores were also adjusted for $Tcell_{inf}$GEP. Adjustment for $Tcell_{inf}$GEP was performed to understand the additional explanatory value that any of the non-$Tcell_{inf}$GEP signatures had for clinical outcome—an approach equivalent to evaluating the association between clinical outcome and the residuals of consensus signatures after detrending for their relationship with the $Tcell_{inf}$GEP. *p-values* for the 10 non-$Tcell_{inf}$GEP and mIHC cell phenotypes were adjusted for multiplicity; *p*-values for the $Tcell_{inf}$GEP signature and TMB scores were not adjusted for multiplicity due to prior validation in pan-tumor datasets [11,12,18,19].

For the $Tcell_{inf}$GEP signature, positive associations were hypothesized and one-sided *p*-values were calculated (prespecified significance level, $\alpha = 0.05$). For the 10 non-$Tcell_{inf}$GEP signatures, negative associations were hypothesized (except for proliferation, which had a hypothesized positive association) and one-sided multiplicity-adjusted *P* values were calculated (prespecified significance level, $\alpha = 0.10$); this level of significance was used due to limitations in power. To determine the general discriminatory ability of $Tcell_{inf}$GEP, the association between $Tcell_{inf}$GEP as a continuous variable and response was evaluated using the area under the receiver operating characteristic curve (AUROC). The impact of the non-$Tcell_{inf}$GEP signatures on efficacy estimates was assessed using the signature-specific $Tcell_{inf}$GEP-adjusted median (≥median vs <median).

The association of TMB (log_{10} scale) as a continuous variable with clinical outcomes was evaluated using one-sided *P* values at a prespecified significance level of $\alpha = 0.05$. To

determine the general discriminatory ability of TMB, the association between TMB as a continuous variable and response was evaluated using the AUROC. The impact of TMB on efficacy estimates was assessed using a prespecified cutoff of 175 mutations/exome (≥175 vs <175 mutations/exome).

For the association between densities of prespecified subsets of mIHC cell phenotypes and clinical outcomes, a positive association was hypothesized; one-sided *p*-values were adjusted for multiplicity (prespecified significance level, $\alpha = 0.05$). To determine the general discriminatory ability of the prespecified subsets of mIHC cell phenotypes in the tumor compartment, as well as other selected mIHC cell phenotypes in the tumor compartment, stromal compartment, and the overall TME, the association between their densities and response was evaluated using the AUROC.

The evaluation of the correlation of select biomarkers was performed using Spearman's correlation analysis of matched dual biomarker data. The database cutoff for clinical data used in this study was February 2, 2018.

3. Results

3.1. Patients

In the overall study population of KEYNOTE-100, median follow-up duration, defined as the time from first dose to death or database cutoff, was 16.9 months (range, 8.5–18.5) [6]. Of the 376 patients who received ≥1 dose of pembrolizumab monotherapy, 317 (84.3%) had evaluable RNA-sequencing data, 293 (77.9%) had evaluable WES data, 125 (33.3%) had mIHC activated T-cell panel data, and 124 (33.0%) had mIHC modified myeloid panel data. Baseline characteristics in the RNA, WES, and mIHC populations were generally

similar to those of the total study population (Table 1). Efficacy data for the RNA, WES, and mIHC populations are presented in Table 1.

3.2. Association of RNA-sequencing gene expression signatures with clinical outcomes

When $Tcell_{inf}$GEP was evaluated as a continuous variable, no significant association with clinical outcomes was observed (Table 2). $Tcell_{inf}$GEP trended higher in responders (n = 28) than nonresponders (n = 289; Fig. 1A) and the AUROC for $Tcell_{inf}$GEP discriminating between responders and nonresponders was 0.57 (95% confidence interval [CI], 0.44–0.71; Fig. 1B). When non-$Tcell_{inf}$GEP signatures were evaluated as continuous variables, no significant association with ORR was observed.

The $Tcell_{inf}$GEP-adjusted glycolysis and hypoxia signatures were negatively associated with longer-term clinical outcomes (glycolysis: PFS, adjusted p = 0.019, OS, adjusted p = 0.085; hypoxia: PFS, adjusted p = 0.064), although the magnitude of the associations was limited. When evaluating efficacy estimates using the median of the $Tcell_{inf}$GEP-adjusted glycolysis or hypoxia signatures to define subgroups for illustrative purposes, the glycolysis ≥median (n = 159) versus glycolysis <median (n = 158) subgroups had comparable median PFS estimates (9.0 weeks [95% CI, 9.0–not estimable (NE)] versus 9.6 weeks [95% CI, 9.1–NE]; Supplementary Fig. S3A). Similarly, the hypoxia ≥median (n = 158) versus hypoxia <median (n = 159) subgroups had comparable median PFS estimates (9.0 weeks [95% CI, 8.9–NE] versus 9.6 weeks [95% CI, 9.1–NE]; Supplementary Fig. S3B). No significant associations were observed for other non-$Tcell_{inf}$GEP signatures and longer-term clinical outcomes after multiplicity adjustment (Table 2). The distribution of all 10 non-$Tcell_{inf}$GEP signature scores after adjusting for $Tcell_{inf}$GEP showed an overall trend toward numerically higher medians in nonresponders than in responders (Fig. 2).

3.3. Association of WES TMB with clinical outcomes

When TMB was evaluated as a continuous variable, no significant association with clinical outcome was observed (ORR, $p = 0.556$; PFS, $p = 0.834$; OS, $p = 0.891$). TMB score distributions were similar between responders ($n = 23$) and nonresponders ($n = 270$; Fig. 1C) and the AUROC for TMB discriminating between responders and nonresponders was 0.50 (95% CI, 0.36–0.63; Fig. 1D). When evaluating efficacy estimates based on a prespecified cutoff for the TMB ≥175 mutations/exome ($n = 12$) versus TMB <175 mutations/exome ($n = 281$) subgroups, ORR was 16.7% (95% CI, 2.1–48.4) versus 7.5% (95% CI, 4.7–11.2), median PFS was 18.0 weeks (95% CI, 8.9–NE) versus 9.1 weeks (95% CI, 9.1–NE), and median OS was 76.4 weeks (95% CI, 56.1–NE) versus 83.3 weeks (95% CI, 73.0–NE).

3.4. Association of mIHC cell phenotypes with clinical outcomes

When the prespecified subset of mIHC cell phenotypes in the tumor compartment was evaluated as continuous variables, significant positive associations were observed for ORR and the $CD11c^+$ (adjusted $p = 0.025$) and $CD11c^+/MHCII^-/CD163^-/CD68^-$ (adjusted $p = 0.013$) phenotypes (Table 2). The densities of $CD11c^+$, $CD11c^+/MHCII^-/CD163^-/CD68^-$, and $CD11c^+/CD163^+$ phenotypes trended greater in responders than nonresponders, whereas the density of $CD11c^+/MHCII^+/CD163^-/CD68^-$ trended greater in nonresponders than responders (Fig. 3). The AUROC for the phenotypes discriminating between responders and nonresponders was 0.59 (95% CI, 0.45–0.73) for $CD11c^+$, 0.61 (95% CI, 0.47–0.75) for $CD11c^+/MHCII^-/CD163^-/CD68^-$, 0.44 (95% CI, 0.31–0.56) for $CD11c^+/MHCII^+/CD163^-/CD68^-$, and 0.58 (95% CI, 0.44–0.71) for $CD11c^+/CD163^+$ (Fig. 3).

We further descriptively evaluated select mIHC phenotypes Foxp3$^+$, CD8$^+$/GB$^+$/Ki67$^+$, and CD11c$^+$/MHCII$^-$/CD163$^-$/CD68$^-$ by spatial localization; these phenotypes all showed high discriminatory ability in the tumor compartment relative to other phenotypes based on AUROC. The densities of Foxp3$^+$, CD8$^+$/GB$^+$/Ki67$^+$, and CD11c$^+$/MHCII$^-$/CD163$^-$/CD68$^-$ phenotypes in the tumor compartment were greater in responders than nonresponders (Fig. 4A); the AUROC for the phenotypes discriminating between responders and nonresponders was 0.67 (95% CI, 0.54–0.80) for Foxp3$^+$, 0.65 (95% CI, 0.52–0.77) for CD8$^+$/GB$^+$/Ki67$^+$, and 0.61 (95% CI, 0.47–0.75) for CD11c$^+$/MHCII$^-$/CD163$^-$/CD68$^-$ (Supplementary Fig. S4A). The densities of Foxp3$^+$, CD8$^+$/GB$^+$/Ki67$^+$, and CD11c$^+$/MHCII$^-$/CD163$^-$/CD68$^-$ phenotypes in the stromal compartment were greater in responders than nonresponders (Fig. 4B); the AUROC for the phenotypes discriminating between responders and nonresponders was 0.69 (95% CI, 0.57–0.81) for Foxp3$^+$, 0.62 (95% CI, 0.50–0.74) for CD8$^+$/GB$^+$/Ki67$^+$, and 0.66 (95% CI, 0.54–0.79) for CD11c$^+$/MHCII$^-$/CD163$^-$/CD68$^-$ (Supplementary Fig. S4B). The densities of Foxp3$^+$, CD8$^+$/GB$^+$/Ki67$^+$, and CD11c$^+$/MHCII$^-$/CD163$^-$/CD68$^-$ phenotypes in the overall TME trended greater in responders than nonresponders (Fig. 4C); the AUROC for the phenotypes discriminating between responders and nonresponders was 0.70 (95% CI, 0.58–0.82) for Foxp3$^+$, 0.64 (95% CI, 0.52–0.76) for CD8$^+$/GB$^+$/Ki67$^+$, and 0.66 (95% CI, 0.53–0.78) for CD11c$^+$/MHCII$^-$/CD163$^-$/CD68$^-$ (Supplementary Fig. S4C).

When the select mIHC cell phenotype densities in the tumor compartment were evaluated by PFI/TFI, densities of Foxp3$^+$, CD8$^+$/GB$^+$/Ki67$^+$, and CD11c$^+$/MHCII$^-$/CD163$^-$/CD68$^-$ phenotypes trended greater in responders than nonresponders at PFI/TFI cutoffs of 3 to <6 months and 6 to 12 months (Supplementary Fig. S5). There was a positive correlation between phenotype densities and PD-L1 CPS for Foxp3$^+$ (Spearman's $\rho = 0.57$), CD8$^+$/GB$^+$/Ki67$^+$ (Spearman's $\rho = 0.53$), and CD11c$^+$/MHCII$^-$/CD163$^-$/CD68$^-$ (Spearman's

$\rho = 0.39$) phenotypes (Supplementary Fig. S6). Similarly, there was a positive correlation between phenotype densities and $Tcell_{inf}GEP$ for the $Foxp3^+$ (Spearman's $\rho = 0.61$), $CD8^+/GB^+/Ki67^+$ (Spearman's $\rho = 0.61$), and $CD11c^+/MHCII^-/CD163^-/CD68^-$ (Spearman's $\rho = 0.41$) phenotypes (Supplementary Fig. S7).

4. Discussion

In this retrospective prespecified exploratory analysis of KEYNOTE-100, the $Tcell_{inf}GEP$-adjusted glycolysis and hypoxia signatures were significantly negatively associated with longer-term clinical outcomes of pembrolizumab when tested on the continuous scale. Further, analysis by the predetermined TMB cutoff of 175 mutations/exome (equivalent to 10 mutations/megabase) showed that response to pembrolizumab was higher in the TMB ≥175 mutations/exome subgroup compared with the TMB <175 mutations/exome subgroup. Additionally, the densities of $CD11c^+$ and $CD11c^+/MHCII^-/CD163^-/CD68^-$ phenotypes in the tumor compartment were significantly positively associated with ORR to pembrolizumab when tested on the continuous scale.

Although a trend for higher $Tcell_{inf}GEP$ signature scores was observed in responders compared with nonresponders, $Tcell_{inf}GEP$ tested as a continuous variable was not significantly associated with ORR, PFS, and OS. Similarly, none of the non-$Tcell_{inf}GEP$ signatures tested were significantly associated with objective response, although angiogenesis and stroma/EMT/TGF-β signatures had distribution trends for responders versus nonresponders, which appear consistent with exploratory studies in the pan-tumor [12,19] and tumor-specific [20, 21] settings. Unlike the $Tcell_{inf}GEP$, the $Tcell_{inf}GEP$-adjusted glycolysis and hypoxia gene expression signatures showed significant negative associations with PFS and/or OS, suggesting that these signatures are potential biomarkers of worse clinical outcomes. Although the magnitude of the associations was limited, this observation is

consistent with the known association of tumor hypoxia with therapy resistance and poor outcomes in patients with cancer [22], and so may reflect an association that is not a predictive biomarker of pembrolizumab resistance but rather a general prognostic finding. Likewise, the glycolysis pathway is recognized as a potential antitumor therapy target [23-26] given that tumor cell phenotypes are characterized by an altered energy metabolism, involving the preferential dependence on the glycolysis pathway for energy in an oxygen-dependent manner [23, 25].

Our evaluation of efficacy estimates based on a prespecified TMB (determined by WES) cutoff of 175 mutations/exome showed numerically higher ORR, numerically longer median PFS, and numerically shorter median OS in patients with TMB ≥175 mutations/exome versus <175 mutations/exome. These observations for ORR and PFS are consistent with findings in the pan-tumor setting, which showed that a TMB of ≥175 mutations/exome is associated with response to pembrolizumab [11] and lends further credence to the potential utility of the TMB ≥175 mutations/exome for selecting patients who may respond effectively to pembrolizumab in the clinical setting. However, the small sample size in the TMB ≥175 mutations/exome subgroup (n = 12) may introduce variability to the findings of this subgroup analysis, including the contrasting observations with the efficacy estimates for OS versus PFS and ORR.

Studies in other tumor types have shown that the presence of certain cell phenotypes frequently detected in the TME are significantly correlated with outcomes of pembrolizumab [27-30]. Consistent with such findings, our evaluation of the prespecified subset of mIHC phenotypes showed that the densities of $CD11c^+$ and $CD11c^+/MHCII^-/CD163^-/CD68^-$ phenotypes were associated with improved response to pembrolizumab in the advanced ROC setting. Given the complex roles of immune cell infiltrates in the TME and the possibility of

subset heterogeneity within each type of immune cell [31], further studies are needed to elucidate the potential mechanisms through which $CD11c^+$ and $CD11c^+/MHCII^-/CD163^-/CD68^-$ phenotype enrichment may improve response in this setting as well as validate the role of the $CD11c^+$ and $CD11c^+/MHCII^-/CD163^-/CD68^-$ phenotypes as biomarkers of response to pembrolizumab.

When the densities of select mIHC phenotypes were evaluated across the tumor and stromal compartments and the overall TME, a similar trend of higher densities of $Foxp3^+$, $CD8^+/GB^+/Ki67^+$, and $CD11c^+/MHCII^-/CD163^-/CD68^-$ phenotypes in responders versus nonresponders was observed, suggesting that these phenotypes may serve as biomarkers of response regardless of the tissue compartment examined. When these phenotypes were further evaluated by PFI/TFI, higher densities of $Foxp3^+$, $CD8^+/GB^+/Ki67^+$, and $CD11c^+/MHCII^-/CD163^-/CD68^-$ phenotypes were observed in responders than nonresponders at PFI/TFI cutoffs of 3 to <6 months and 6 to 12 months; an important caveat is that this observation may be limited by the small sample size of the subgroups and by high variability across patients.

This exploratory analysis is the largest study of an anti–PD-1 monotherapy in patients with advanced ROC, and the study population had a good distribution of prior lines of therapies. Another strength of this analysis is that the evaluable RNA-sequencing (84.3%) and TMB (77.9%) populations comprised a high proportion of the total study population; thus, inferences drawn from these respective datasets are largely representative of the KEYNOTE-100 study population. However, the single-arm nature of the KEYNOTE-100 study precludes an interpretation of the predictive role of the molecular determinants evaluated in this exploratory study; a comparator arm is needed for validation. Other limitations include the low number of responders in the overall population; the low prevalence of patients with TMB

≥175 mutations/exome (4.1%; 12/293; equivalent to ≥10 mutations/megabase); and the selection of the mIHC population to include responders as well as the selected mIHC population comprising only 33.2% of the overall treated patients in the KEYNOTE-100 study.

In conclusion, this exploratory analysis from the KEYNOTE-100 study did not find evidence for associations between gene expression signatures on the continuous scale and clinical outcomes to pembrolizumab. Although this analysis suggests that lower levels of $Tcell_{inf}$GEP-adjusted glycolysis and hypoxia gene expression signatures, as determined by univariate analysis, may be associated with improved longer-term outcomes, there was no evidence of an association between these 2 gene expression signatures and objective response. Currently, several clinical trials investigating the efficacy of combination therapy targeting PD-1/L1 and hypoxia- or glycolysis-related gene targets in ovarian cancer are ongoing: a phase II study (NCT03827837) is investigating the tyrosine kinase inhibitor famitinib in combination with the anti–PD-1 monoclonal antibody camrelizumab in patients with advanced tumors (including ROC) and another phase II study (NCT04068974) is investigating the combination of the tyrosine kinase inhibitor apatinib (which suppresses glycolysis by targeting vascular endothelial growth factor receptor-2 [32]) and camrelizumab in patients with recurrent platinum-resistant ovarian cancer. In addition, we also show that the TMB ≥175 mutations/exome subgroup had better clinical outcomes to pembrolizumab versus TMB <175 mutations/exome and that higher densities of $CD11c^+$ and $CD11c^+/MHCII^-/CD163^-/CD68^-$ phenotypes representing myeloid cell populations may be associated with improved outcomes of pembrolizumab in patients with advanced ROC. With respect to the mIHC cell phenotype evaluation, $CD8^+$ signatures appeared to show stronger association with clinical response than $CD11^+$ signatures.

Acknowledgements

The authors thank the patients and their families and caregivers as well as the primary investigators and site personnel for participating in the study. The authors also thank Jennifer Yearley and Assieh Saadatpour of Merck Sharp & Dohme LLC, a subsidiary of Merck & Co., Inc., Rahway, NJ, USA for study support. Medical writing and/or editorial assistance was provided by Obinna T. Ezeokoli, PhD, and Holly C. Cappelli, PhD, CMPP, of ApotheCom (Yardley, PA, USA). This assistance was funded by Merck Sharp & Dohme LLC, a subsidiary of Merck & Co., Inc., Rahway, NJ, USA.

Funding

This work was supported by Merck Sharp & Dohme LLC, a subsidiary of Merck & Co., Inc., Rahway, NJ, USA. The funder participated in the study design, data analysis and interpretation, and manuscript writing. All authors had full access to the data and had final responsibility for the decision to submit for publication.

Declaration of Competing Interest

J.A. Ledermann reports receiving research grants from AstraZeneca and Merck/MSD; lecture fees from Clovis Oncology, AstraZeneca, Neopharm, GSK and MSD/Merck; and advisory board fees from AstraZeneca, GSK, Artios Pharma, Clovis Oncology, ImmunoGen, Mersana, Bristol Myers Squibb, Nuvation, Ellipses Pharma, VBL Therapeutics, Eisai, Regeneron, and Immagene, outside of the submitted work.

R. Shapira-Frommer reports receiving support with medical writing for the submitted work from MSD; a research grant from MSD; consulting fees paid to her from MSD and Clovis Oncology; payment or honoraria for lectures, presentations, speakers bureaus, manuscript

writing or educational events paid to her from MSD, Bristol Myers Squibb, Roche, AstraZeneca, Sanofi, Medison Pharma, Neopharm, and Novartis; participation on a data safety monitoring board or advisory board for MSD (received personal fee), Novartis (received personal fee), and AstraZeneca (unpaid); and a role in the ENGOT early phase study group (unpaid), outside of the submitted work.

A.D. Santin reports grants or contracts paid to his institution from Genentech, Immunomedics, Gilead, Merck, Boehringer Ingelheim, and Tesaro; consulting fees paid to him from Merck, Eisai, and R-Pharm US; and participation on a data safety monitoring board or advisory board for Merck, Eisai, and R-PHARM US, outside of the submitted work.

A.S. Lisyanskaya reports no disclosures.

S. Pignata reports receiving payment or honoraria for lectures, presentations, speakers' bureaus, manuscript writing, or educational events from MSD, GSK, Roche, AstraZeneca, and Clovis Oncology, outside of the submitted work.

I. Vergote reports contracted research via KU Leuven to his institution from Oncoinvent AS; corporate-sponsored research to his institution from Amgen and Roche; consulting fees paid to him from Agenus, Akesobio, AstraZeneca, Bristol Myers Squibb, Deciphera Pharmaceuticals, Eisai, Elevar Therapeutics, Exelixis, Roche, Genmab, GSK, ImmunoGen, Jazz Pharmaceuticals, Karyopharm Therapeutics, Mersana, MSD, Novocure, Novartis, Oncoinvent, OncXerna, Regeneron, Sanofi, Seagen, Sotio, Verastem Oncology, and Zentalis; and travel support to himself from Karyopharm Therapeutics, Genmab, and Novocure, outside of the submitted work.

F. Raspagliesi reports receiving grants or contracts from GSK, MSD, and AstraZeneca; payment or honoraria for lectures, presentations, speakers' bureaus, manuscript writing or educational events from GSK, MSD, and AstraZeneca; and support for attending meetings and/or travel from GSK, outside of the submitted work.

G.S. Sonke reports payments to his institution for inclusion of trial subjects and medical writing support, all from MSD, for the submitted work; institutional research support from Agendia, AstraZeneca, Merck, Novartis, Roche, and Seagen; and consulting fees paid to his institution from Biovica, Novartis, and Seagen, outside of the submitted work.

M. Birrer reports no disclosures.

D.M. Provencher reports receiving payment or honoraria for lectures, presentations, speakers' bureaus, manuscript writing or educational events from AstraZeneca and GSK and participation on a data safety monitoring board or advisory board for GSK, outside of the submitted work.

J. Sehouli reports receiving consulting fees from Roche, GSK, Tesaro, Novocure, Clovis Oncology, MSD, Merck, Pfizer, and Astra Zeneca; payment or honoraria for lectures, presentations, speakers' bureaus, manuscript writing, or educational events from Roche, GSK, Tesaro, Novocure, Clovis, MSD, Merck, Pfizer, Astra Zeneca, and Eisai; support for attending meetings and/or travel from Roche, GSK, Tesaro, and AstraZeneca; participation on a data safety monitoring board or advisory board for Roche, GSK, Tesaro, Novocure, Clovis Oncology, MSD, Merck, Pfizer, AstraZeneca, Eisai, and PharmaMar; and roles on/as the council of ESGO), president of NOGGO, president of PARSGO, speaker of the Ovarian Cancer Commission (AGO), and delegate to GCIG, outside of the submitted work.

N. Colombo reports receiving medical writing support from MSD for the submitted work; grants or contracts paid to her from MSD, Roche, and GSK; consulting fees paid to her from MSD, Roche, GSK, and AstraZeneca; payment or honoraria for lectures, presentations, speakers bureaus, manuscript writing or educational events to her from AstraZeneca, GSK, Novartis, Clovis Oncology, and MSD; support for attending meetings and/or travel from AstraZeneca, MSD, and GSK; participation on a data safety monitoring board or advisory board for AstraZeneca, Clovis Oncology, Eisai, GSK, ImmunoGen, Mersana, MSD/Merck,

Nuvation Bio, OncXerna Therapeutics, Pfizer, Pieris, and Roche; and unpaid roles for ACTO Onlus and ESMO Guidelines Committee, outside of the submitted work.

A. González-Martín reports receiving grants or contracts from Roche, GSK, GEICO, and CCUN; consulting fees paid to him from Alkermes, Amgen, AstraZeneca, Clovis Oncology, Genmab, GSK, HederaDx, ImmunoGen, Illumina, Mersana, MSD, Novartis, Novocure, Oncoinvent, PharmaMar, Roche, SOTIO, Sutro Biopharma, Seagen, and Takeda; consulting fees paid to him from Alkermes, Amgen, AstraZeneca, Clovis Oncology, Genmab, GSK, HederaDx, ImmunoGen, Illumina, Mersana, MSD, Novartis, Novocure, Oncoinvent, PharmaMar, Roche, SOTIO, Sutro Biopharma, Seagen, and Takeda; payment or honoraria for lectures, presentations, speakers bureaus, manuscript writing, or educational events paid to him from GSK, Clovis, AstraZeneca, MSD, Mersana, and Roche; support for attending meetings and/or travel paid to him from AstraZeneca/MSD and GSK; and unpaid roles as president of GEICO and ENGOT, outside of the submitted work.

A. Oaknin reports grants or contracts paid to her institution from AbbVie Deutschland, Advaxis Inc., Aeterna Zentaris, Amgen, Aprea Therapeutics AB, Bristol Myers Squibb, Clovis Oncology Inc, Eisai, Roche, ImmunoGen, MSD de España S.A., Millennium Pharmaceuticals, PharmaMar SA, Regeneron Pharmaceuticals, and Tesaro; consulting fees paid to her from Agenus, AstraZeneca, Clovis Oncology, Corcept Therapeutics, Deciphera Pharmaceuticals, Eisai, EMD Serono, Roche, Genmab, GSK, ImmunoGen, Itheos, MSD de España, S.A., Mersana Therapeutics, Novocure, PharmaMar, prIME Oncology, Roche, Sattucklabs, Seagen, Sutro Biopharma, and Tesaro; payment or honoraria for lectures, presentations, speakers bureaus, manuscript writing or educational events from ESMO, Edizioni Minerva Medica SpA, and Doctaforum Servicios S.L; support for attending meetings and/or travel paid to her from AstraZeneca, PharmaMar, and Roche; and payment to her for participation on a data safety monitoring board or advisory board from Agenus,

AstraZeneca, Clovis Oncology, Corcept Therapeutics, Deciphera Pharmaceuticals, Eisai, EMD Serono, Roche, Genmab, GSK, ImmunoGen, Itheos, MSD de España S.A., Mersana Therapeutics, Novocure, PharmaMar, prIME Oncology, Roche, Sattucklabs, Seagen, Sutro Biopharma, and Tesaro, outside of the submitted work.

P. B. Ottevanger reports receiving support for manuscript writing and provision of study patients from MSD for the submitted work.

V. Rudaitis reports no disclosures.

J. Kobie is an employee of Merck Sharp & Dohme LLC, a subsidiary of Merck & Co., Inc., Rahway, NJ, USA, and has stock in Merck & Co., Inc., Rahway, NJ, USA.

M. Nebozhyn is an employee of Merck Sharp & Dohme LLC, a subsidiary of Merck & Co., Inc., Rahway, NJ, USA, and has stock in Merck & Co., Inc., Rahway, NJ, USA.

M. Edmondson is an employee of Merck Sharp & Dohme LLC, a subsidiary of Merck & Co., Inc., Rahway, NJ, USA.

Y. Sun is an employee of Merck Sharp & Dohme LLC, a subsidiary of Merck & Co., Inc., Rahway, NJ, USA and has stock in Merck & Co., Inc., Rahway, NJ, USA.

R. Cristescu is an employee of Merck Sharp & Dohme LLC, a subsidiary of Merck & Co., Inc., Rahway, NJ, USA and has stock in Merck & Co., Inc., Rahway, NJ, USA; and reports a pending patent (WO 2020/167619) related to the application of Angiogenesis and mMDSC gene expression-based biomarker of tumor response to PD-1 antagonists.

P. Jelinic is an employee of Merck Sharp & Dohme LLC, a subsidiary of Merck & Co., Inc., Rahway, NJ, USA.

S.M. Keefe is an employee of Merck Sharp & Dohme LLC, a subsidiary of Merck & Co., Inc., Rahway, NJ, USA, and has stock in Merck & Co., Inc., Rahway, NJ, USA.

U.A. Matulonis reports consulting fees paid to her from Merck, GSK, and AstraZeneca; payment made to her from Med Learning Group for her role on the committee on endometrial

cancer, which involved creation of the entire lecture and slides; payment made to her for lectures, presentations, speakers bureaus, manuscript writing, or educational events from Research to Practice; payments made to her for participation on the advisory board for Allarity, NextCure, Trillium, Agenus, ImmunoGen, Novartis, Boehringer Ingelheim, Rivkin Foundation, Ovarian Cancer Research Alliance, Clearity Foundation, MorphoSys, and CureLab; and payments for participation on a data safety monitoring board for Alkermes and Symphogen, outside of the submitted work.

Author Contributions

Conceptualization: JAL, JS, PJ, SMK, and UAM.

Methodology: PJ and SMK.

Investigation: JAL, ADS, ASL, SP, IV, FR, GSS, MB, DMP, JS, NC, AG-M, AO, PBO, VR, YS, RC, PJ, and UAM.

Data curation: JAL, ADS, ASL, SP, IV, FR, GSS, MB, DMP, JS, NC, AG-M, AO, PBO, VR, YS, RC, PJ, and UAM.

Formal analysis: IV, JS, JS, MN, ME, YS, RC, PJ, SMK, and UAM.

Validation: JAL, RS-F, ADS, ASL, IV, FR, GSS, MB, JS, NC, AG-M, AO, PBO, JS, MN, ME, YS, RC, PJ, SMK, and UAM.

Writing – original draft: JAL, JS, JS, YS, RC, PJ, SMK, and UAM.

Writing – review and editing: JAL, RS-F, ADS, ASL, SP, IV, FR, GSS, MB, DMP, JS, NC, AG-M, AO, and UAM.

Data sharing

Merck Sharp & Dohme LLC, a subsidiary of Merck & Co., Inc., Rahway, NJ, USA (MSD) is committed to providing qualified scientific researchers access to anonymized data and

clinical study reports from the company's clinical trials for the purpose of conducting legitimate scientific research. MSD is also obligated to protect the rights and privacy of trial participants and, as such, has a procedure in place for evaluating and fulfilling requests for sharing company clinical trial data with qualified external scientific researchers. The MSD data-sharing website (available at: http://engagezone.msd.com/ds_documentation.php) outlines the process and requirements for submitting a data request. Applications will be promptly assessed for completeness and policy compliance. Feasible requests will be reviewed by a committee of MSD subject matter experts to assess the scientific validity of the request and the qualifications of the requestors. In line with data privacy legislation, submitters of approved requests must enter into a standard data-sharing agreement with MSD before data access is granted. Data will be made available for request after product approval in the United States and the European Union or after product development is discontinued. There are circumstances that may prevent MSD from sharing requested data, including country or region-specific regulations. If the request is declined, it will be communicated to the investigator. Access to genetic or exploratory biomarker data requires a detailed, hypothesis-driven statistical analysis plan that is collaboratively developed by the requestor and MSD subject matter experts; after approval of the statistical analysis plan and execution of a data-sharing agreement, MSD will either perform the proposed analyses and share the results with the requestor or will construct biomarker covariates and add them to a file with clinical data that is uploaded to an analysis portal so that the requestor can perform the proposed analyses.

References

[1] Siegel RL, Miller KD, Fuchs HE, Jemal A. Cancer statistics, 2022. CA Cancer J Clin. 2022;72:7-33.

[2] Colombo N, Sessa C, du Bois A, Ledermann J, McCluggage WG, McNeish I, et al. ESMO-ESGO consensus conference recommendations on ovarian cancer: pathology and molecular biology, early and advanced stages, borderline tumours and recurrent disease†. Ann Oncol. 2019;30:672-705.

[3] KEYTRUDA (pembrolizumab) injection, for intravenous use. Merck Sharp & Dohme Corp.: Whitehouse Station, NJ; 2022.

[4] JEMPERLI (dostarlimab-gxly) injection, for intravenous use. GlaxoSmithKline: Research Triangle Park, NC; 2022.

[5] Varga A, Piha-Paul S, Ott PA, Mehnert JM, Berton-Rigaud D, Morosky A, et al. Pembrolizumab in patients with programmed death ligand 1-positive advanced ovarian cancer: analysis of KEYNOTE-028. Gynecol Oncol. 2019;152:243-50.

[6] Matulonis UA, Shapira-Frommer R, Santin AD, Lisyanskaya AS, Pignata S, Vergote I, et al. Antitumor activity and safety of pembrolizumab in patients with advanced recurrent ovarian cancer: results from the phase II KEYNOTE-100 study. Ann Oncol. 2019;30:1080-7.

[7] Hamanishi J, Mandai M, Ikeda T, Minami M, Kawaguchi A, Murayama T, et al. Safety and Antitumor Activity of Anti-PD-1 Antibody, Nivolumab, in Patients With Platinum-Resistant Ovarian Cancer. J Clin Oncol. 2015;33:4015-22.

[8] Disis ML, Taylor MH, Kelly K, Beck JT, Gordon M, Moore KM, et al. Efficacy and Safety of Avelumab for Patients With Recurrent or Refractory Ovarian Cancer: Phase 1b Results From the JAVELIN Solid Tumor Trial. JAMA Oncol. 2019;5:393-401.

[9] Hamanishi J, Takeshima N, Katsumata N, Ushijima K, Kimura T, Takeuchi S, et al. Nivolumab versus gemcitabine or pegylated liposomal doxorubicin for patients with platinum-resistant ovarian cancer: open-label, randomized trial in Japan (NINJA). J Clin Oncol. 2021;39:3671-81.

[10] Aurora-Garg D, Albright A, Qiu P, Li Y, Liu X, Fabrizio D, et al. Large-scale evaluation of concordance of genomic scores in whole exome sequencing and foundation medicine comprehensive genomic platform across cancer types. J Immunother Cancer. 2019;7:172.

[11] Cristescu R, Aurora-Garg D, Albright A, Xu L, Liu XQ, Loboda A, et al. Tumor mutational burden predicts the efficacy of pembrolizumab monotherapy: a pan-tumor retrospective analysis of participants with advanced solid tumors. J Immunother Cancer. 2022;10.

[12] Cristescu R, Nebozhyn M, Zhang C, Albright A, Kobie J, Huang L, et al. Transcriptomic determinants of response to Pembrolizumab monotherapy across solid tumor types. Clin Cancer Res. 2022;28:1680-9.

[13] Singh L, Muise ES, Bhattacharya A, Grein J, Javaid S, Stivers P, et al. ILT3 (LILRB4) promotes the immunosuppressive function of tumor-educated human monocytic myeloid-derived suppressor cells. Mol Cancer Res. 2021;19:702-16.

[14] Veglia F, Perego M, Gabrilovich D. Myeloid-derived suppressor cells coming of age. Nat Immunol. 2018;19:108-19.

[15] Gebhardt C, Sevko A, Jiang H, Lichtenberger R, Reith M, Tarnanidis K, et al. Myeloid cells and related chronic inflammatory factors as novel predictive markers in melanoma treatment with ipilimumab. Clin Cancer Res. 2015;21:5453-9.

[16] Meyer C, Cagnon L, Costa-Nunes CM, Baumgaertner P, Montandon N, Leyvraz L, et al. Frequencies of circulating MDSC correlate with clinical outcome of melanoma patients treated with ipilimumab. Cancer Immunol Immunother. 2014;63:247-57.

[17] Groth C, Hu X, Weber R, Fleming V, Altevogt P, Utikal J, et al. Immunosuppression mediated by myeloid-derived suppressor cells (MDSCs) during tumour progression. Br J Cancer. 2019;120:16-25.

[18] Ayers M, Lunceford J, Nebozhyn M, Murphy E, Loboda A, Kaufman DR, et al. IFN-γ–related mRNA profile predicts clinical response to PD-1 blockade. J Clin Invest. 2017;127:2930-40.

[19] Cristescu R, Mogg R, Ayers M, Albright A, Murphy E, Yearley J, et al. Pan-tumor genomic biomarkers for PD-1 checkpoint blockade-based immunotherapy. Science. 2018;362:eaar3593.

[20] Bellmunt J, de Wit R, Fradet Y, Climent MA, Petrylak DP, Lee JL, et al. Putative biomarkers of clinical benefit with pembrolizumab in advanced urothelial cancer: Results From the KEYNOTE-045 and KEYNOTE-052 landmark trials. Clin Cancer Res. 2022;28:2050–60.

[21] Haddad R, Seiwert TY, Chow LQM, Gupta S, Weiss J, Gluck I, et al. Influence of tumor mutational burden, inflammatory gene expression profile, and PD-L1 expression on response to pembrolizumab in head and neck squamous cell carcinoma. J. Immunother Cancer. 2022;10:e003026.

[22] Muz B, de la Puente P, Azab F, Azab AK. The role of hypoxia in cancer progression, angiogenesis, metastasis, and resistance to therapy. Hypoxia (Auckl). 2015;3:83-92.

[23] Yu L, Chen X, Sun X, Wang L, Chen S. The glycolytic switch in tumors: How many players are involved? J Cancer. 2017;8:3430-40.

[24] Chen XS, Li LY, Guan YD, Yang JM, Cheng Y. Anticancer strategies based on the metabolic profile of tumor cells: therapeutic targeting of the Warburg effect. Acta Pharmacol Sin. 2016;37:1013-9.

[25] Ganapathy-Kanniappan S, Geschwind JF. Tumor glycolysis as a target for cancer therapy: progress and prospects. Mol Cancer. 2013;12:152.

[26] Granchi C, Minutolo F. Anticancer agents that counteract tumor glycolysis. ChemMedChem. 2012;7:1318-50.

[27] Tumeh PC, Harview CL, Yearly JH, Shintaku IP, Taylor EJM, Robert L, et al. PD-1 blockade induces responses by inhibiting adaptive immune resistance. Nature. 2014;515:568-71.

[28] Loi S, Winer E, Lipatov O, Im S-A, Goncalves A, Cortes J, et al. Abstract PD5-03: Relationship between tumor-infiltrating lymphocytes (TILs) and outcomes in the KEYNOTE-119 study of pembrolizumab vs chemotherapy for previously treated metastatic triple-negative breast cancer (mTNBC). Can Res. 2020;80(suppl 4):PD5-03-PD503-. DOI:10.1158/1538-7445.SABCS19-PD5-03.

[29] Loi S, Adams S, Schmid P, Cortés J, Cescon DW, Winer EP, et al. Abstract LBA13. Relationship between tumor infiltrating lymphocyte (TIL) levels and response to pembrolizumab (pembro) in metastatic triple-negative breast cancer (mTNBC): Results from KEYNOTE-086. Ann Oncol. 2017;28 (suppl 5):668.

[30] Schmid P, Park YH, Muñoz-Couselo E, Kim SB, Sohn J, Im SA, et al. Effects of pembrolizumab on the tumor microenvironment (TME) after one presurgery treatment cycle in patients with triple-negative breast cancer (TNBC): phase 1b KEYNOTE-173 study. In: 338, editor. J Immunother Cancer. 2021;9(suppl 2):A364.

[31] Shui IM, Liu XQ, Zhao Q, Kim ST, Sun Y, Yearley JH, et al. Baseline and post-treatment biomarkers of resistance to anti-PD-1 therapy in acral and mucosal melanoma: an observational study. J Immunother Cancer. 2022;10:e004879.

[32] Chen L, Cheng X, Tu W, Qi Z, Li H, Liu F, et al. Apatinib inhibits glycolysis by suppressing the VEGFR2/AKT1/SOX5/GLUT4 signaling pathway in ovarian cancer cells. Cell Oncol (Dordr). 2019;42:679-90.

TABLES

Table 1. Baseline characteristics and clinical outcomes in the analysis populations. Data are n (%) unless otherwise specified.

	Overall study population *N* = 376	RNA-sequencing population *n* = 317	WES population *n* = 293	mIHC activated T-cell panel population *n* = 125	mIHC modified myeloid panel population *n* = 124
Cohort					
A	285 (75.8)	240 (75.7)	219 (74.7)	93 (74.4)	92 (74.2)
B	91 (24.2)	77 (24.3)	74 (25.3)	32 (25.6)	32 (25.8)
PD-L1 status[a]					
CPS <1	139 (37.0)	117 (36.9)	102 (34.8)	39 (31.2)	38 (30.6)
CPS ≥1	202 (53.7)	175 (55.2)	161 (54.9)	75 (60.0)	75 (60.5)
CPS ≥10	83 (22.1)	73 (23.0)	63 (21.5)	35 (28.0)	35 (28.2)
Platinum sensitivity[b]					
Refractory (PFI, ≤4 weeks)	4 (1.1)	3 (0.9)	2 (0.7)	2 (1.6)	2 (1.6)
Resistant (PFI, >1 to <6 months)	141 (37.5)	120 (37.9)	109 (37.2)	48 (38.4)	48 (38.7)
Partially sensitive (PFI, 6–12 months)	128 (34.0)	104 (32.8)	98 (33.4)	43 (34.4)	42 (33.9)
Sensitive (PFI, >12 months)	18 (4.8)	17 (5.4)	16 (5.5)	8 (6.4)	8 (6.5)
ECOG performance status					
0	242 (64.4)	198 (62.5)	189 (64.5)	87 (69.6)	86 (69.4)
1	134 (35.6)	119 (37.5)	104 (35.5)	38 (30.4)	38 (30.6)
Histology[c]					
High-grade serous	283 (75.3)	236 (74.4)	216 (73.7)	106 (84.8)	105 (84.7)
Endometrioid	28 (7.4)	22 (6.9)	24 (8.2)	0 (0)	0 (0)
Low-grade serous	21 (5.6)	0 (0)	0 (0)	0 (0)	0 (0)
Clear cell	19 (5.1)	17 (5.4)	17 (5.8)	12 (9.6)	12 (9.7)
Other	25 (6.6)	42 (13.2)	36 (12.3)	7 (5.6)	7 (5.6)
Outcomes					

ORR[d]	30 (8.0)	28 (8.8)	23 (7.8)	28 (22.4)	28 (22.6)
PFS, median (95% CI), weeks	9.1 (9.1–9.4)	9.1 (9.1–9.4)	9.1 (9.1–9.4)	9.0 (9.0–9.1)	9.0 (9.0–9.1)
OS, median (95% CI), weeks	81.1 (73.9–NE)	NE (74.9–NE)	80.0 (73.0–NE)	NE (75.9–NE)	NE (75.9–NE)

Abbreviations: CI, confidence interval; CPS, combined positive score; ECOG, Eastern Cooperative Oncology Group; mIHC, multiplex immunohistochemistry; NE, not estimable; ORR, objective response rate; OS, overall survival; PD-L1, programmed cell death ligand 1; PFI, platinum-free interval; PFS, progression-free survival.

[a]Biomarker analyses used CPS as a continuous variable; results may differ from CPS as a categorical variable. PD-L1 status data was missing for 35 (9.3%), 25 (7.9%), 30 (10.2%), 11 (8.8%), and 11 (8.9%) patients in the overall, RNA-sequencing, WES, mIHC activated T-cell panel, and mIHC modified myeloid panel populations, respectively.

[b]Platinum sensitivity was determined as “other” in 85 (22.6%), 73 (23.0%), 68 (23.2%), 24 (19.2%), and 24 (19.4%) patients in the overall, RNA-sequencing, WES, mIHC activated T-cell panel, and mIHC modified myeloid panel populations, respectively.

[c]Not specified as low- or high-grade serous or listed as papillary serous; unclassified or listed as adenocarcinoma or carcinoma; or transitional.

[d]Confirmed complete or partial response per RECIST v1.1 by blinded independent central review.

Table 2. Association *p*-values[a] between RNA-sequencing gene expression signatures (*n* = 317) and prespecified mIHC cell phenotype densities in the tumor compartment (*n* = 124) and clinical outcomes.

Molecular determinants	ORR per RECIST v1.1	PFS per RECIST v1.1	OS
Gene expression signatures			
$Tcell_{inf}$GEP	0.172	0.163	0.590
Adjusted for $Tcell_{inf}$GEP			
Angiogenesis	0.673	0.780	0.989
Glycolysis	0.673	**0.019**	**0.085**
gMDSC	0.673	0.999	0.989
Hypoxia	0.673	**0.064**	0.266
mMDSC	0.673	0.999	0.989
MYC	0.673	0.129	0.989
Proliferation	0.673	0.999	0.989
RAS	0.528	0.692	0.989
Stroma/EMT/TGFβ	0.673	0.999	0.989
WNT	0.673	0.999	0.989
mIHC cell phenotypes			
$CD11c^+$	**0.025**	0.273	0.182
$CD11c^+/MHCII^+/CD163^-/CD68^-$	0.419	0.526	0.597
$CD11c^+/MHCII^-/CD163^-/CD68^-$	**0.013**	0.167	0.182
$CD11c^+/CD163^+$	0.128	0.526	0.322

Abbreviations: ECOG, Eastern Cooperative Oncology Group; EMT, epithelial-to-mesenchymal transition; gMDSC, granulocytic myeloid-derived suppressor cell; mMDSC, monocytic myeloid-derived suppressor cells; ORR, objective response rate; OS, overall survival; PFS, progression-free survival; RECIST v1.1, Response Evaluation Criteria in Solid Tumors version 1.1; $Tcell_{inf}$GEP, T-cell–inflamed gene expression profile; TGF-β, transforming growth factor-beta.

All models include additional covariates of ECOG performance status (all gene expression signatures and mIHC cell phenotypes) and $Tcell_{inf}$GEP (non-$Tcell_{inf}$GEP signatures only).

Positive associations were hypothesized for $Tcell_{inf}$GEP and proliferation signatures and mIHC cell phenotypes; negative associations were hypothesized for the non-$Tcell_{inf}$GEP signatures except for proliferation. Bolded *p*-values indicate multiplicity-adjusted statistical significance (mIHC cell phenotypes, $\alpha = 0.05$; non-$Tcell_{inf}$GEP signatures, $\alpha = 0.10$).

[a]One-sided Wald test for nominal or multiplicity-adjusted *p*-values for signatures using logistic regression (ORR) or Cox proportional hazards regression (PFS; OS).

FIGURES

Fig. 1. Response status and AUROC for (A-B) $Tcell_{inf}GEP$ and (C-D) TMB.

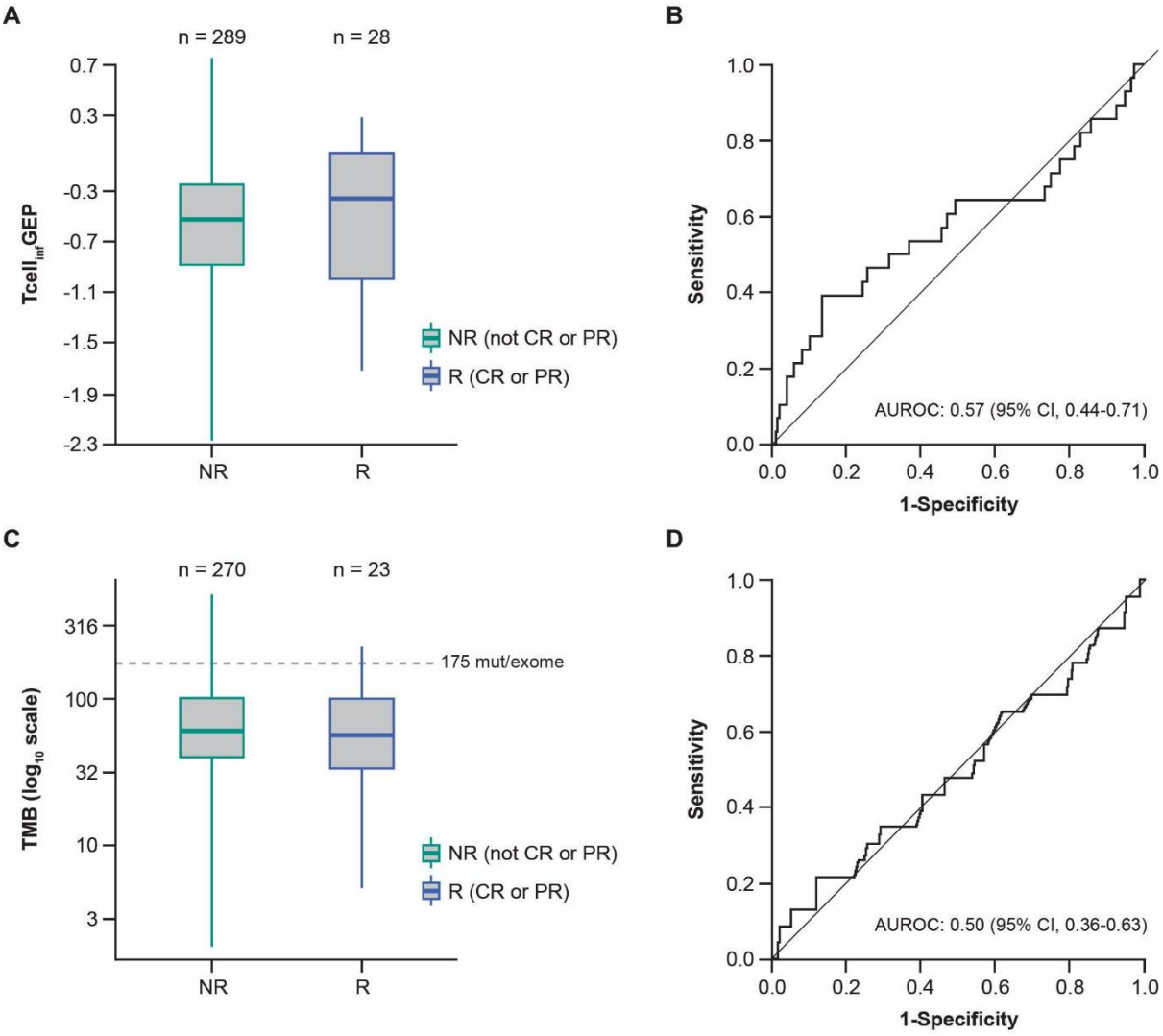

Abbreviations: AUROC, area under the receiver operating characteristic curve; CR, complete response; NR, nonresponders; PR, partial response; R, responders; $Tcell_{inf}GEP$, T-cell–inflamed gene expression profile; TMB, tumor mutational burden.

Fig. 2. Association of non-Tcell$_{inf}$GEP signatures adjusted for the Tcell$_{inf}$GEP with response.

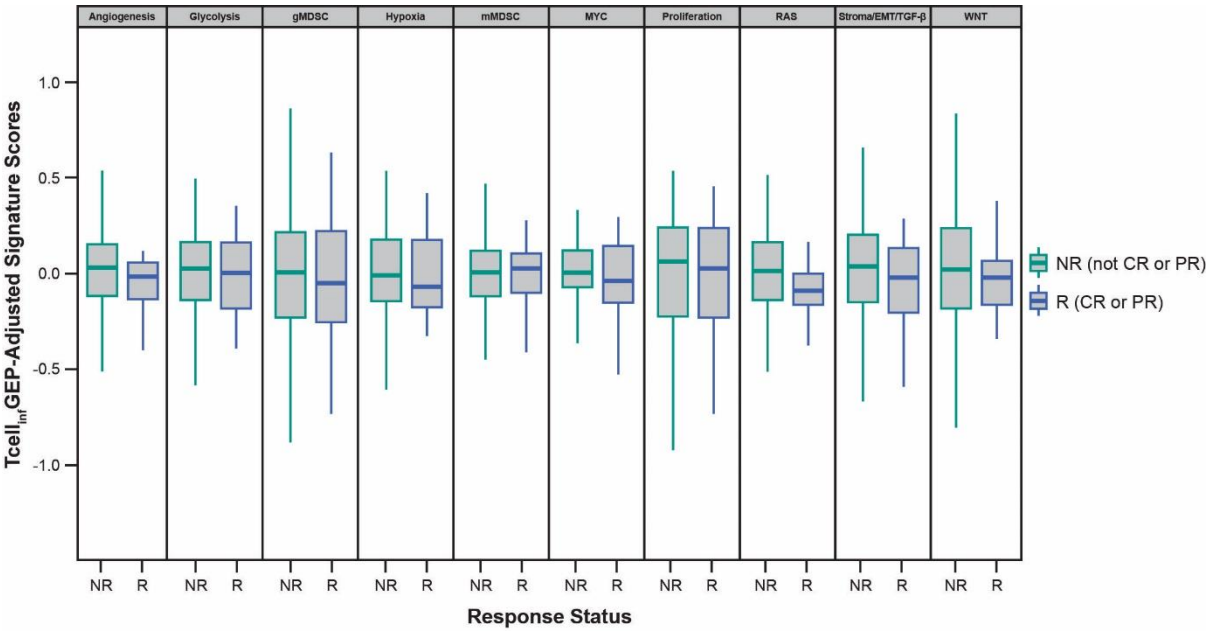

Abbreviations: CR, complete response; EMT, epithelial-to-mesenchymal transition; gMDSC, granulocytic myeloid-derived suppressor cells; mMDSC, monocytic myeloid-derived suppressor cells; NR, nonresponders; PR, partial response; R, responders; Tcell$_{inf}$GEP, T-cell–inflamed gene expression profile; TGF-β, transforming growth factor-beta.

Fig. 3. Response status and AUROC for prespecified mIHC cell phenotype densities in the tumor compartment. (A-B) $CD11c^+$, (C-D) $CD11c^+/MHCII^-/CD163^-/CD68^-$, (E-F) $CD11c^+/MHCII^+/CD163^-/CD68^-$, and (G-H) $CD11c^+/CD163^+$.

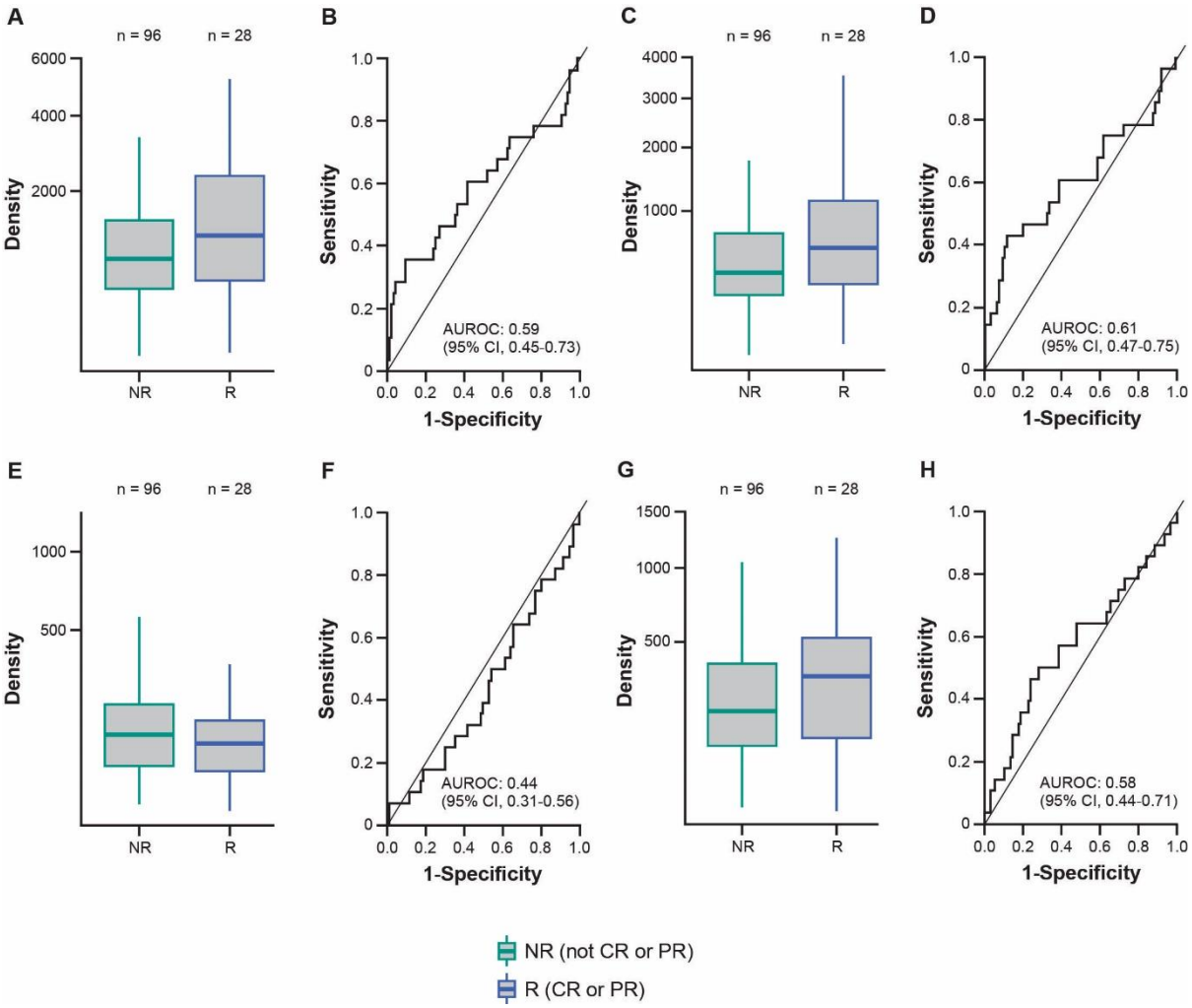

Abbreviations: AUROC, area under the receiver operating characteristic curve; CR, complete response; mIHC, multiplex immunohistochemistry; NR, nonresponders; PR, partial response; R, responders.

Fig. 4. Response status for Foxp3^{+}, CD8^{+}/GN^{+}/Ki67^{+}, and CD11c^{+}/MHCII$^{–}$/CD163$^{–}$/CD68$^{–}$ mIHC densities by spatial localization. (A) Tumor compartment. (B) Stromal compartment. (C) Overall TME.

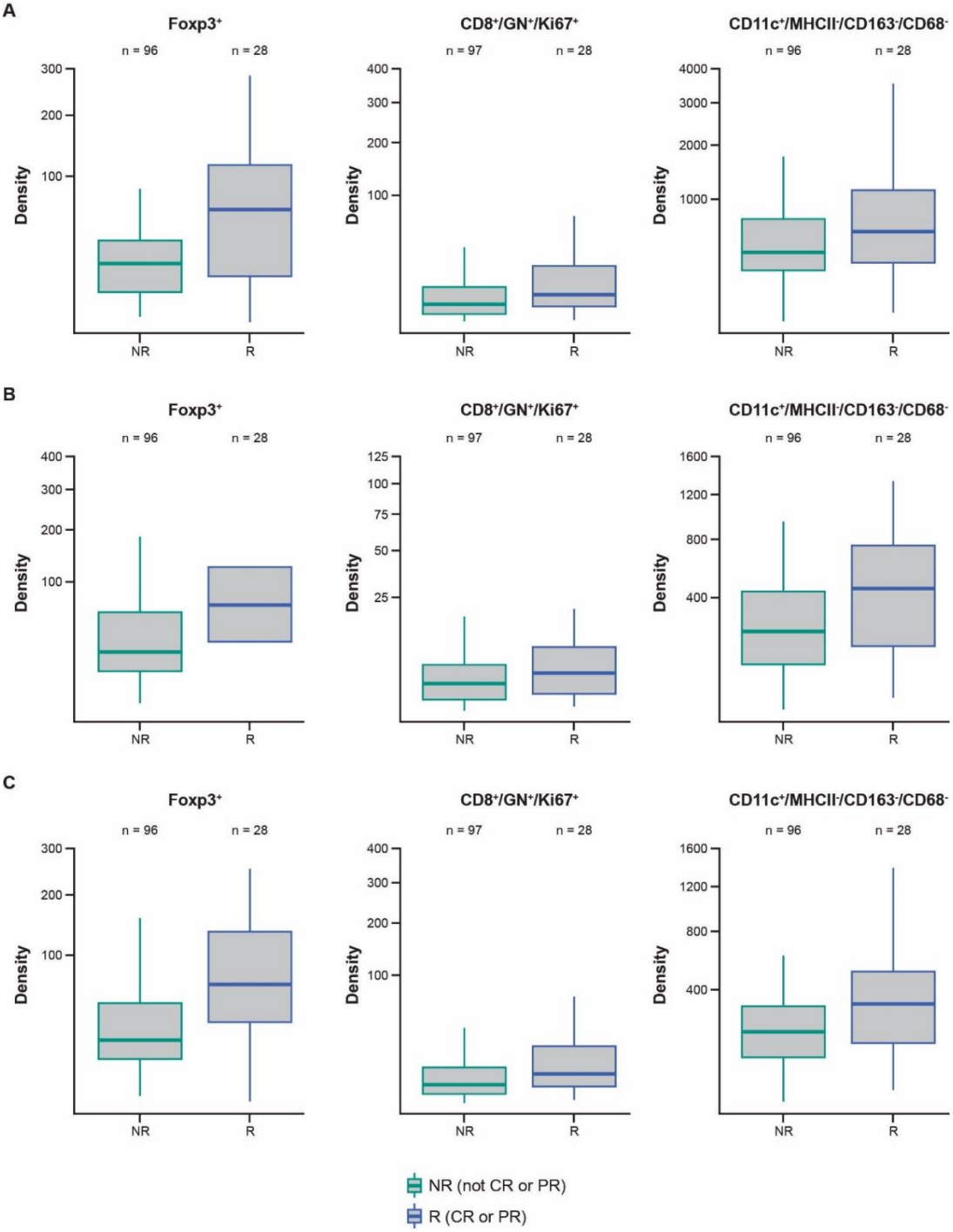

Abbreviations: CR, complete response; mIHC, multiplex immunohistochemistry; NR, nonresponders; PR, partial response; R, responders; TME, tumor microenvironment.

Supplementary materials for: Molecular determinants of clinical outcomes of pembrolizumab in recurrent ovarian cancer: exploratory analysis of KEYNOTE-100

Authors: J.A. Ledermann et al

Supplementary Text 1. mIHC staining and quantitative imaging

Briefly, 5 μm sections were cut from formalin-fixed paraffin-embedded tissue blocks and baked at 60°C for 1 h, then deparaffinized and rehydrated with serial passage through changes of xylene and graded ethanol. Thereafter, slides were subjected to heat-induced epitope retrieval in 1× Target Retrieval Solution (Agilent Technologies Inc., Carpinteria, CA). Endogenous peroxidase in tissues was blocked by incubation of slides in 3% hydrogen peroxide solution followed by protein blocking with PKI buffer (Akoya Biosciences, Marlborough, MA). Six-plex staining was conducted on a Bond RX stainer (Leica Biosystems, Buffalo Grove, IL) using tyramide signal amplification (TSA)–based Opal multiplexing reagents (Akoya Biosciences). Each primary antibody (Supplementary **Table S1**) was incubated for 60 minutes, followed by Opal polymer horseradish peroxidase secondary and TSA-conjugated Opal fluorophore application (Akoya Biosciences). Antibody stripping was performed using epitope retrieval 1 buffer (Leica Biosystems) after each staining cycle. Nuclei were detected using Spectral DAPI (Akoya Biosciences) and slides were cover slipped for scanning (21). Stained slides were scanned using the Vectra Polaris Imaging System (Akoya Biosciences) at 20× magnification. Image tiles were deconvoluted using the inForm software (Akoya Biosciences) and stitched into whole slide images using Halo software (Indica Labs, Albuquerque, NM), followed by quantitative analysis. Tumor-containing regions were defined using manual annotations on scanned hematoxylin and eosin whole-slide images in Halo software (Indica Labs). The annotations of tumor-containing

regions were transferred to the serial mIHC images using internal custom-developed software. Using Random Forest classifier in Halo (v3.0.311.337), tumor-containing regions were segmented into tumor and stromal compartments.

TABLES

Supplementary Table S1. Primary antibodies used for mIHC.

Antibody	Host/Clone	Supplier	Paired opal fluorophore
CD103	Rabbit/EPR4166	Abcam, Boston, MA	Opal480
CD39	Mouse/2B10	LifeSpan Biosciences, Seattle, WA	Opal520
Granzyme B	Mouse/GZB01	Thermo Fisher Scientific, Fremont, CA	Opal570
CD8	Mouse/C8/144B	Agilent, Bayonne, NJ	Opal620
Cytokeratin	Mouse/AE1/AE3	Agilent, Bayonne, NJ	Opal690
Ki67	Mouse/MIB-1	Agilent, Bayonne, NJ	Opal780
MHCII (HLA-DR)	Mouse/LN3	Thermo Scientific, Fremont, CA	Opal690
Foxp3	Mouse/236A/E7	Abcam, Boston, MA	Opal480
CD163	Mouse/10D6	Thermo Fisher Scientific, Fremont, CA	Opal520
Fibroblast activation protein	Rabbit/EPR20021	Abcam, Boston, MA	Opal570
CD68	Mouse/KP1	Agilent, Bayonne, NJ	Opal620
CD11c	Mouse/5D11	Leica Biosystems, Deer Park, IL	Opal780

Abbreviation: mIHC, multiplex immunohistochemistry.

FIGURES

Supplementary Fig. S1. Representative image for the 6-plex activated T-cell panel (CD103/CD39/Granzyme B/CD8/Cytokeratin/Ki67).

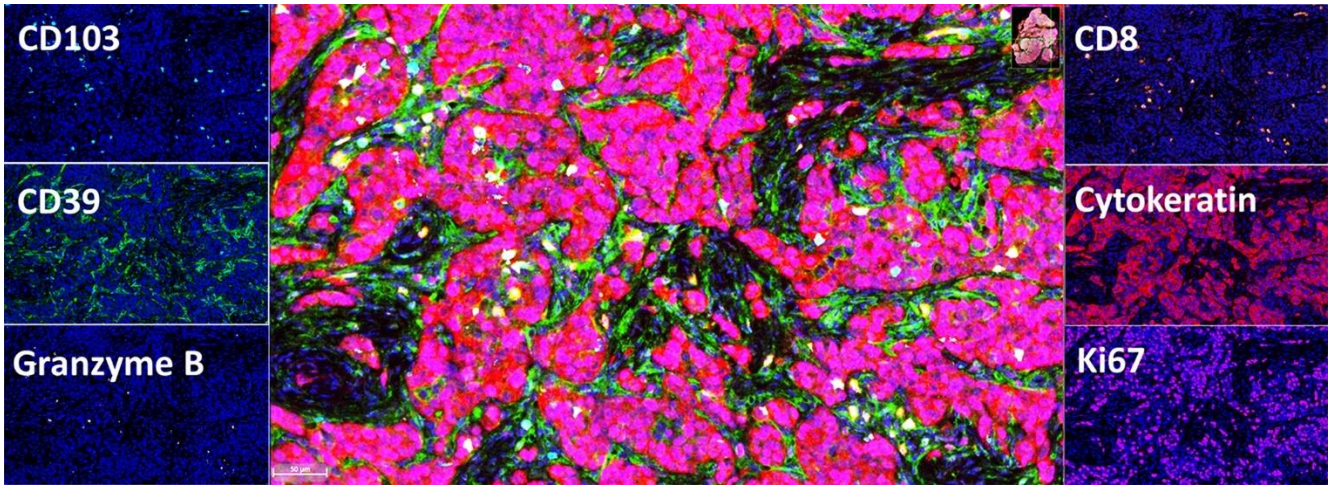

Key (related cell types): CD103 and CD39, tumor reactive CD8 T cells; Granzyme B, activated T/natural killer cells; CD8, cytotoxic T cells; Ki67, proliferation; Cytokeratin, Epithelium.

Supplementary Fig. S2. Representative image for the 6-plex myeloid/Stroma/Treg panel (CD68/CD163/CD11c/ MHCII/FAP/FoxP3).

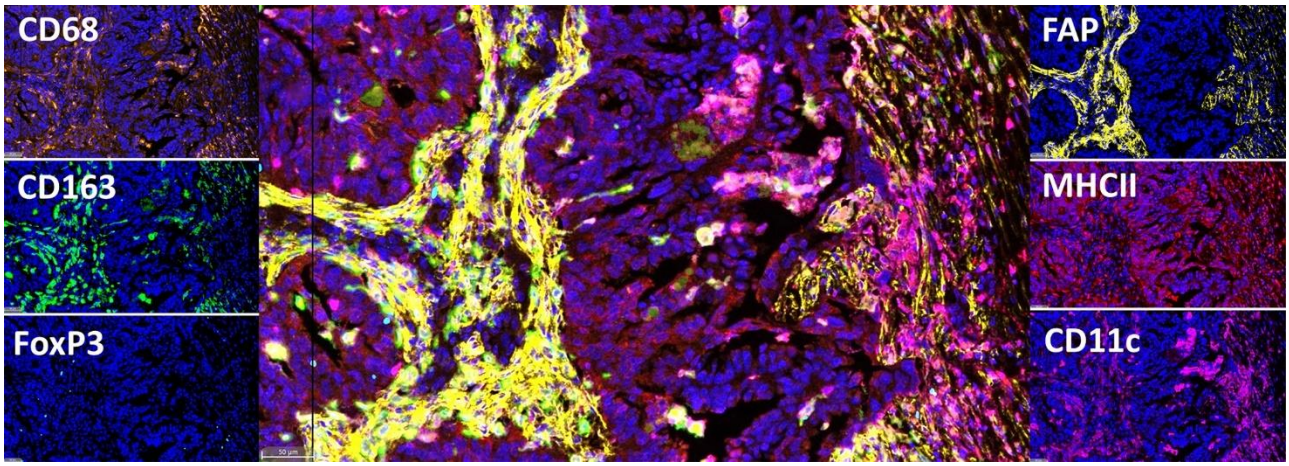

Key (related cell types): CD11c, dendritic cells and macrophages; CD68, macrophages; CD163, M2 enriched macrophages; FAP, cancer-associated fibroblasts; FoxP3, regulatory T cells; MHCII, antigen-presenting cells.

Supplementary Fig. S3. Progression-free survival by median cutoff for $Tcell_{inf}$GEP-adjusted (A) glycolysis and (B) hypoxia gene expression signatures.

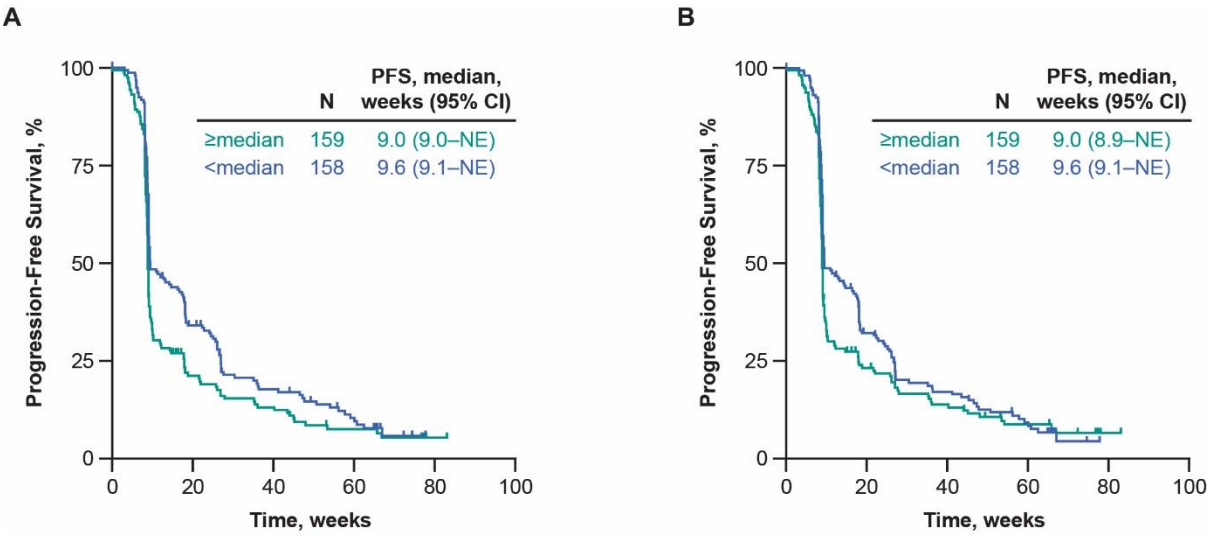

Abbreviations: CI, confidence interval; NE, not estimable; PFS, progression-free survival; $Tcell_{inf}$GEP, T-cell–inflamed gene expression profile.

Supplementary Fig. S4. AUROC for Foxp3^{+}, CD8^{+}/GN^{+}/Ki67^{+}, and CD11c^{+}/MHCII^{-}/CD163^{-}/CD68^{-} mIHC densities a by spatial localization. (A) Tumor compartment. (B) Stromal compartment. (C) Overall tumor microenvironment.

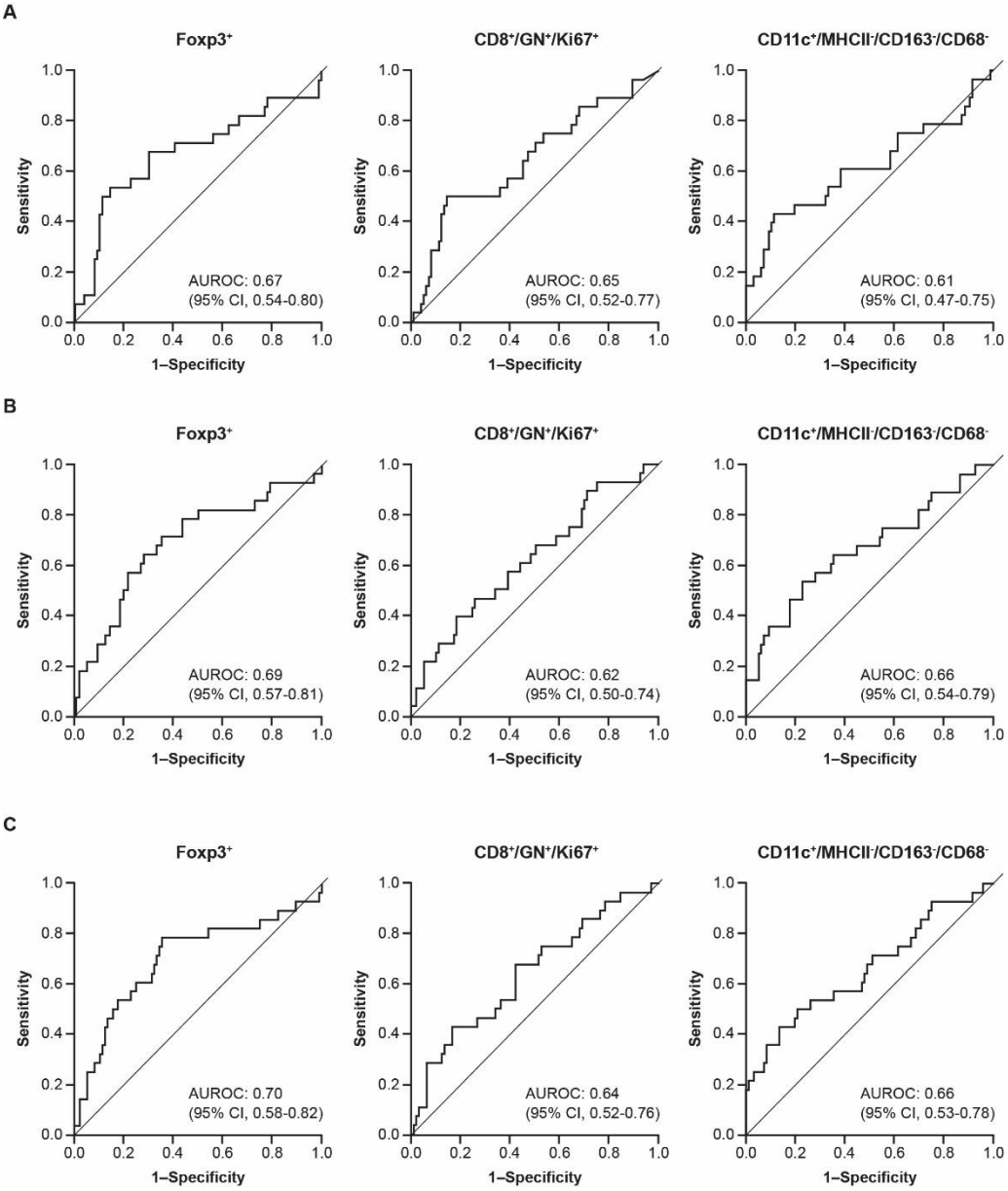

Abbreviations: AUROC, area under the receiver operating characteristic curve; CI, confidence interval; mIHC, multiplex immunohistochemistry.

Supplementary Fig. S5. Response status for select mIHC cell phenotype densities in tumor compartment by PFI/TFI. (A) Foxp3^{+}, (B) CD8^{+}/GB^{+}/Ki67^{+}, and (C) CD11c^{+}/MHCII^{-}/CD163^{-}/CD68^{-}.

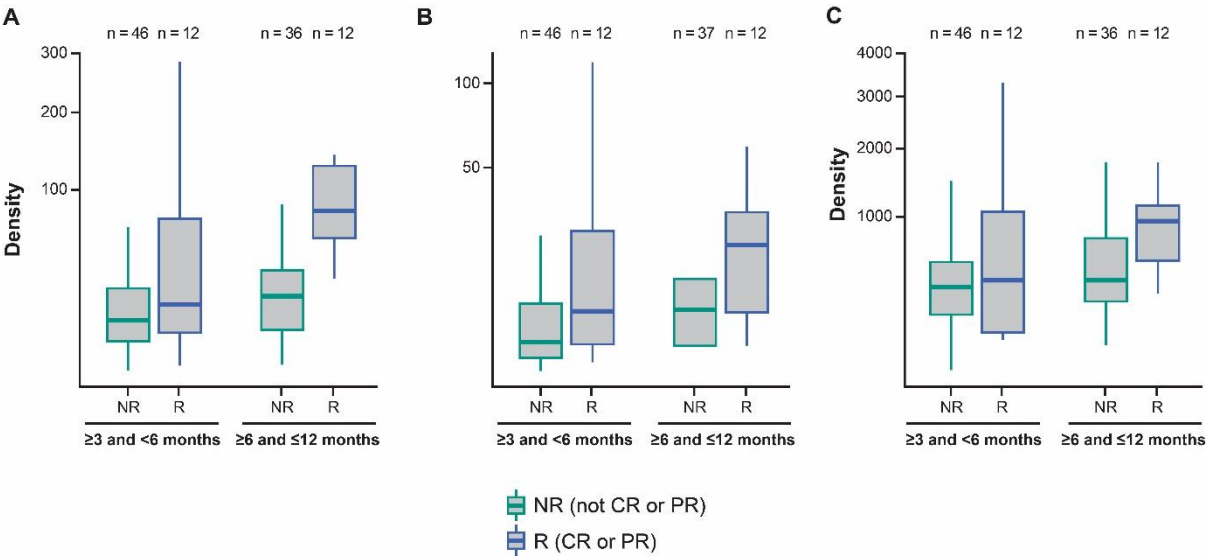

Abbreviations: CR, complete response; mIHC, multiplex immunohistochemistry; NR, nonresponders; PFI, platinum-free interval; PR, partial response; R, responders; TFI, treatment-free interval.

Supplementary Fig. S6. Joint effect of select mIHC cell phenotypes densities in tumor compartment and PD-L1 CPS on response. (A) $Foxp3^{+}$, (B) $CD8^{+}/GB^{+}/Ki67^{+}$, and (C) $CD11c^{+}/MHCII^{-}/CD163^{-}/CD68^{-}$.

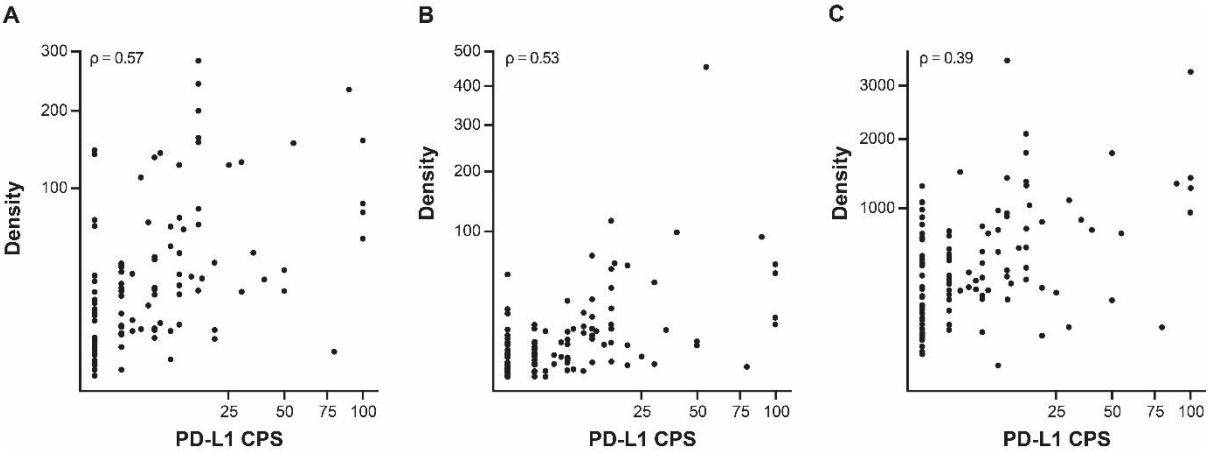

Abbreviations: CPS, combined positive score; mIHC, multiplex immunohistochemistry; PD-L1, programmed death ligand 1.

Supplementary Fig. S7. Joint effect of select mIHC cell phenotype densities in tumor compartment and $Tcell_{inf}GEP$ on response. (A) $Foxp3^+$, (B) $CD8^+/GB^+/Ki67^+$, and (C) $CD11c^+/MHCII^-/CD163^-/CD68^-$.

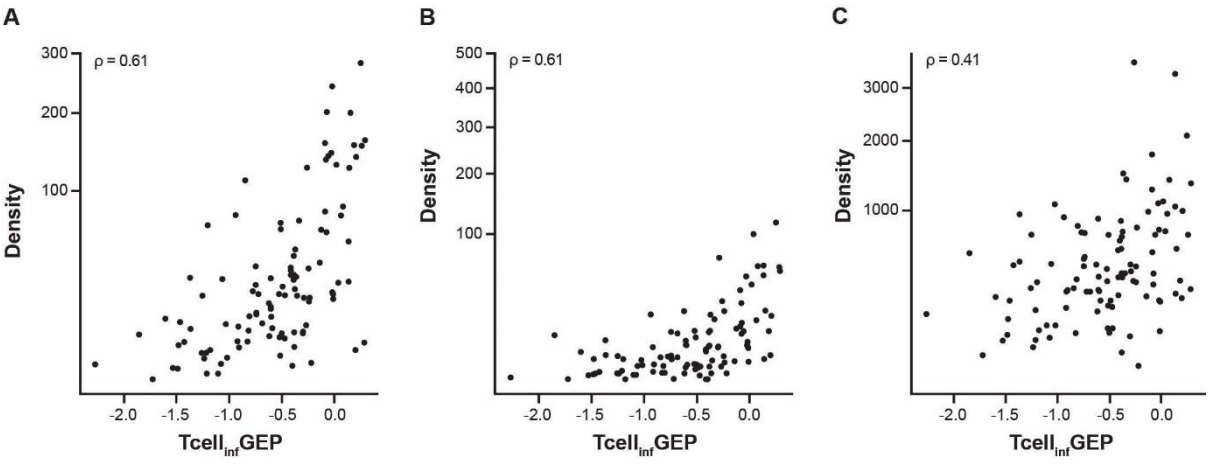

Abbreviations: mIHC, multiplex immunohistochemistry; $Tcell_{inf}GEP$, T-cell–inflamed gene expression profile.